

Strange hadron production in a quark combination model in Au+Au collisions at energies available at the BNL Relativistic Heavy Ion Collider

Jun Song ¹, Xiao-feng Wang,² Hai-hong Li,¹ Rui-qin Wang,² and Feng-lan Shao ^{2,*}

¹*Department of Physics, Jining University, Shandong 273155, China*

²*School of Physics and Physical Engineering, Qufu Normal University, Shandong 273165, China*



(Received 5 August 2020; revised 1 February 2021; accepted 2 March 2021; published 22 March 2021)

We apply a quark combination model to study yield densities and transverse momentum (p_T) spectra of strange (anti)hadrons at midrapidity in central Au+Au collisions at $\sqrt{s_{NN}} = 7.7, 11.5, 19.6, 27, 39,$ and 200 GeV. We show that the experimental data for p_T spectra of (anti)hadrons in these collisions can be systematically described by the equal velocity combination of constituent quarks and antiquarks at hadronization. We obtain the p_T spectra of quarks and antiquarks at hadronization and study their collision energy dependence. We also reproduce the yield densities of hadrons and antihadrons. In particular, we demonstrate that the yield ratios of antihadrons to hadrons $K^-/K^+, \bar{p}/p, \bar{\Lambda}/\Lambda, \bar{\Xi}^+/\Xi^-,$ and $\bar{\Omega}^+/\Omega^-$ simply correlate with each other and their experimental data except $\bar{\Omega}^+/\Omega^-$ at $\sqrt{s_{NN}} = 7.7$ GeV are systematically described by the model. These results suggest that the equal velocity combination mechanism for quarks and antiquarks at hadronization plays an important role for the production of these long-lived hadrons in Au+Au collisions at low RHIC energies ($\sqrt{s_{NN}} \geq 11.5$ GeV).

DOI: [10.1103/PhysRevC.103.034907](https://doi.org/10.1103/PhysRevC.103.034907)

I. INTRODUCTION

Hadron production from final state partons in high-energy collisions is a complex quantum chromodynamics (QCD) process. Due to the difficulty of nonperturbative QCD, phenomenological mechanisms and models have to be applied to describe the production of hadrons at hadronization [1–8]. In relativistic heavy-ion collisions at high RHIC and LHC energies, quark-gluon plasma (QGP) is created in early stage of collisions and the hadronization of QGP can be microscopically described by the quark (re)combination/coalescence mechanism [9–14]. The enhanced ratio of baryon to meson and number of constituent quark scaling for elliptic flows of hadrons at the intermediate transverse momentum (p_T) are typical experimental signals for quark combination mechanism at hadronization and have been widely observed in relativistic heavy-ion collisions [15–22].

In our recent studies in high-multiplicity events in pp and p -Pb collisions at LHC energies where the mini-QGP is possibly created and rescattering of hadrons is weak, we found an interesting quark number scaling property for p_T spectra of hadrons at midrapidity [23,24]. This scaling property is a direct consequence of equal velocity combination (EVC) of constituent quarks and antiquarks at hadronization. Our studies showed that the EVC of up/down, strange and charm quarks can provide a good and systematic description on p_T spectra of light, strange and charm hadrons in ground-state in pp and p -Pb collisions at LHC energies [23–27]. In latest work [28], we further found that the experimental data for p_T spectra of Ω and ϕ at midrapidity in heavy-ion collisions

in a broad collision energy range ($\sqrt{s_{NN}} = 11.5$ – 2760 GeV) also satisfy the quark number scaling property. This is a clear signal of EVC at hadronization even in heavy-ion collisions. Therefore, it is interesting to systematically test this mechanism by production of more hadron species in relativistic heavy-ion collisions.

Recently, STAR collaboration reported their precise experimental data for the production of strange hadrons in Au+Au collisions at $\sqrt{s_{NN}} = 7.7$ – 39 GeV [29]. This provides us a good opportunity to systematically study the EVC mechanism of hadron production in these collisions. In this paper, we apply a quark combination model with EVC to carry out a systematic study on yield densities and p_T spectra of strange hadrons in Au+Au collisions at $\sqrt{s_{NN}} = 7.7, 11.5, 19.6, 27, 39,$ and 200 GeV. We put particular emphasis on the self-consistency of the model in explaining the experimental data for different kinds of hadrons and on the regularity in multihadron production correlations which is sensitive to hadronization mechanism. Taking advantage of precise data for strange hadrons, we also study the strangeness neutralization in the midrapidity region in these collisions. We extract quark p_T distributions at hadronization from data of hadrons and study properties of the relative abundance for strange quarks as the function of collision energy. Furthermore, we discuss the key physics in current quark combination model which are responsible for explaining successfully experimental data of hadronic p_T spectra and yields, and discuss the creation of QGP or the deconfinement at low RHIC energies.

The paper is organized as follows. In Sec. II, we introduce a quark combination model with equal velocity combination approximation. In Sec. III, we study the strangeness neutralization in midrapidity region. In Sec. IV, we show results of p_T spectra for hadrons and compare them with experimental

*shaofl@mail.sdu.edu.cn

data. In Sec. V, we study the split in yield between hadrons and their antiparticles. In Sec. VI, we study properties for the obtained numbers and p_T spectra of quarks at hadronization at different collision energies. The summary and discussion are given at last in Sec. VII.

II. A QUARK COMBINATION MODEL WITH EVC

The quark combination is one of phenomenological mechanisms for hadron production at hadronization. The basic idea of quark combination was first proposed in 1970s [3–5] and has many successful applications in high-energy reactions [6,30–32]. In relativistic heavy-ion collisions, quark combination mechanism is often used to describe the hadron production at QGP hadronization [9–11,13,14,33,34]. Recently, we found that quark combination can also well explain experimental data of hadron production in high-multiplicity pp and p -Pb collisions at LHC energies [23–25,35].

In this paper, inspired by the quark number scaling property of hadronic p_T spectra [23,24,28], we adopt a specific version of quark combination model [23,25]. This model assumes the combination of constituent quarks and antiquarks with equal velocity to form baryons and mesons at hadronization. The unknown nonperturbative dynamics at hadronization are parameterized and their values are assumed to be stable in high-energy reactions and are fixed by experimental data. This model is essentially a statistical model based on the constituent quark degrees of freedom at hadronization and the constituent quark structure of hadrons. It is different from the popular recombination/coalescence models which adopt the Wigner wave function method under instantaneous hadronization approximation [9,10]. The brief description of the model is as follows.

We start from the general formula for the production of the baryon B_j composed of $q_1q_2q_3$ and the production of the meson M_j composed of $q_1\bar{q}_2$ in quark combination mechanism

$$f_{B_j}(p_B) = \int dp_1 dp_2 dp_3 \mathcal{R}_{B_j}(p_1, p_2, p_3; p_B) \times f_{q_1q_2q_3}(p_1, p_2, p_3), \quad (1)$$

$$f_{M_j}(p_M) = \int dp_1 dp_2 \mathcal{R}_{M_j}(p_1, p_2; p_M) f_{q_1\bar{q}_2}(p_1, p_2). \quad (2)$$

Here $f_{q_1q_2q_3}(p_1, p_2, p_3)$ is the joint momentum distribution for q_1 , q_2 , and q_3 . The combination kernel function $\mathcal{R}_{B_j}(p_1, p_2, p_3; p_B)$ denotes the probability density for a given $q_1q_2q_3$ with momenta p_1 , p_2 , and p_3 to combine into a baryon B_j with momentum p_B . It is similar for mesons. We emphasize that Eqs. (1) and (2) are generally suitable for hadron production in momentum space of any dimension. In this paper, we study the one-dimensional transverse momentum (p_T) distribution of hadrons at midrapidity $y = 0$. In this case, p_i simply denotes $p_{T,i}$ and the distribution function $f_h(p)$ denotes the dN_h/dp_T at midrapidity.

The combination functions $\mathcal{R}_{B_j}(p_1, p_2, p_3; p_B)$ and $\mathcal{R}_{M_j}(p_1, p_2; p_M)$ contain the key information of combination dynamics which is not clear at present due to the nonperturbative difficulty of hadronization. In our recent works [23,24,28], we observed an interesting quark number scaling

property for the p_T spectra of hadrons in high-multiplicity pp and p -Pb collisions as well as in heavy-ion collisions. This scaling property supports the combination of constituent quarks and antiquarks with equal velocity. This suggests an effective form for the combination kernel functions, i.e.,

$$\mathcal{R}_{B_j}(p_1, p_2, p_3; p_B) = \kappa_{B_j} \prod_{i=1}^3 \delta(p_i - x_i p_B), \quad (3)$$

$$\mathcal{R}_{M_j}(p_1, p_2; p_M) = \kappa_{M_j} \prod_{i=1}^2 \delta(p_i - x_i p_M). \quad (4)$$

Here, κ_{B_j} and κ_{M_j} are coefficients independent of momentum. Momentum fraction x_i is determined by the masses of constituent quarks because $p_i = m_i \gamma \beta \propto m_i$. Specifically, we have $x_i = m_i/(m_1 + m_2 + m_3)$ for baryon B_j with $x_1 + x_2 + x_3 = 1$ and $x_i = m_i/(m_1 + m_2)$ for meson M_j with $x_1 + x_2 = 1$. m_i is the constituent mass for quark of flavor i . Because the mass of the formed hadron under Eqs. (3) and (4) is the sum of these of constituent quarks, we take constituent masses $m_u = m_d = 0.3$ GeV and $m_s = 0.5$ GeV to properly describe the production of baryons and vector mesons studied in this paper.

The joint momentum distributions $f_{q_1q_2q_3}(p_1, p_2, p_3)$ and $f_{q_1\bar{q}_2}(p_1, p_2)$ generally contain the correlation term caused by, for example, the collective flow formed in system evolution before hadronization in heavy-ion collisions. To obtain analytical and simple expressions for $f_{B_j}(p_B)$ and $f_{M_j}(p_M)$, we take the independent distribution approximation

$$f_{q_1q_2q_3}(p_1, p_2, p_3) = f_{q_1}(p_1) f_{q_2}(p_2) f_{q_3}(p_3), \quad (5)$$

$$f_{q_1\bar{q}_2}(p_1, p_2) = f_{q_1}(p_1) f_{\bar{q}_2}(p_2). \quad (6)$$

Substituting Eqs. (3)–(6) into Eqs. (1) and (2), we obtain

$$f_{B_j}(p_B) = \kappa_{B_j} f_{q_1}(x_1 p_B) f_{q_2}(x_2 p_B) f_{q_3}(x_3 p_B), \quad (7)$$

$$f_{M_j}(p_M) = \kappa_{M_j} f_{q_1}(x_1 p_M) f_{\bar{q}_2}(x_2 p_M). \quad (8)$$

κ_{B_j} and κ_{M_j} carry the information of p_T -independent combination dynamics. To determine their forms, we express momentum distributions of hadrons in another form:

$$f_{B_j}(p_B) = N_{B_j} f_{B_j}^{(n)}(p_B), \quad (9)$$

$$f_{M_j}(p_M) = N_{M_j} f_{M_j}^{(n)}(p_M). \quad (10)$$

N_{B_j} and N_{M_j} are numbers of B_j and M_j , respectively. $f_{B_j}^{(n)}(p_B)$ and $f_{M_j}^{(n)}(p_M)$ are distribution functions normalized to one when integrating over momentum, which can be obtained by those of quarks and antiquarks,

$$f_{B_j}^{(n)}(p_B) = A_{B_j} f_{q_1}^{(n)}(x_1 p_B) f_{q_2}^{(n)}(x_2 p_B) f_{q_3}^{(n)}(x_3 p_B), \quad (11)$$

$$f_{M_j}^{(n)}(p_M) = A_{M_j} f_{q_1}^{(n)}(x_1 p_M) f_{\bar{q}_2}^{(n)}(x_2 p_M). \quad (12)$$

Here, $f_{q_i}^{(n)}(p) = f_{q_i}(p)/N_{q_i}$ is the normalized distribution function of quark q_i . Normalization coefficients A_{B_j} and A_{M_j} are defined as

$$A_{B_j}^{-1} = \int f_{q_1}^{(n)}(x_1 p_B) f_{q_2}^{(n)}(x_2 p_B) f_{q_3}^{(n)}(x_3 p_B) d p_B, \quad (13)$$

$$A_{M_j}^{-1} = \int f_{q_1}^{(n)}(x_1 p_M) f_{\bar{q}_2}^{(n)}(x_2 p_M) d p_M. \quad (14)$$

Substituting Eqs. (11) and (12) into Eqs. (9) and (10) and then comparing them with Eqs. (7) and (8), we obtain

$$N_{B_j} = N_{q_1} N_{q_2} N_{q_3} \frac{\kappa_{B_j}}{A_{B_j}}, \quad (15)$$

$$N_{M_j} = N_{q_1} N_{\bar{q}_2} \frac{\kappa_{M_j}}{A_{M_j}}. \quad (16)$$

From Eqs. (15) and (16), we can read out the physical meaning of κ_{B_j} and κ_{M_j} . It is obvious that κ_{B_j}/A_{B_j} denotes the momentum-integrated probability of $q_1 q_2 q_3$ forming a baryon B_j and κ_{M_j}/A_{M_j} denotes that of $q_1 \bar{q}_2$ forming a meson M_j . Two probabilities can be further decomposed as

$$\frac{\kappa_{B_j}}{A_{B_j}} \equiv P_{q_1 q_2 q_3 \rightarrow B_j} = C_{B_j} N_{\text{iter}} \frac{\bar{N}_B}{N_q^3}, \quad (17)$$

$$\frac{\kappa_{M_j}}{A_{M_j}} \equiv P_{q_1 \bar{q}_2 \rightarrow M_j} = C_{M_j} \frac{\bar{N}_M}{N_q N_{\bar{q}}}. \quad (18)$$

Taking meson, for example, $\bar{N}_M/N_q N_{\bar{q}}$ is used to denote the averaged probability of a $q\bar{q}$ pair forming a meson. Here, $N_q N_{\bar{q}}$ is the all possible number of $q\bar{q}$ pair, where $N_q = N_u + N_d + N_s$ is the number of all quarks and $N_{\bar{q}} = N_{\bar{u}} + N_{\bar{d}} + N_{\bar{s}}$ is that of all antiquarks. \bar{N}_M is the average number of mesons produced by the hadronization of quark system with given quark number N_q and antiquark number $N_{\bar{q}}$. The factor C_{M_j} denotes further sophisticated tune for the production probability of M_j on the basis of the averaged probability $\bar{N}_M/N_q N_{\bar{q}}$. The baryon formula is similar to meson except a factor N_{iter} . This factor is to assure $\sum_{q_1 q_2 q_3} N_{\text{iter}} N_{q_1} N_{q_2} N_{q_3} = N_q^3$ and equals to 1,3,6 for $q_1 q_2 q_3$ with three identical flavors, two identical flavors, and three different flavors, respectively. Finally, we obtain yield formulas of hadrons

$$N_{B_j} = C_{B_j} N_{\text{iter}} N_{q_1} N_{q_2} N_{q_3} \frac{\bar{N}_B}{N_q^3}, \quad (19)$$

$$N_{M_j} = C_{M_j} N_{q_1} N_{\bar{q}_2} \frac{\bar{N}_M}{N_q N_{\bar{q}}}. \quad (20)$$

\bar{N}_B and \bar{N}_M are functions of N_q and $N_{\bar{q}}$ [36],

$$\bar{N}_M = \frac{x}{2} \left[1 - z \frac{(1+z)^a + (1-z)^a}{(1+z)^a - (1-z)^a} \right], \quad (21)$$

$$\bar{N}_B = \frac{xz}{3} \frac{(1+z)^a}{(1+z)^a - (1-z)^a}, \quad (22)$$

$$\bar{N}_{\bar{B}} = \frac{xz}{3} \frac{(1-z)^a}{(1+z)^a - (1-z)^a}, \quad (23)$$

where $x = N_q + N_{\bar{q}}$ and $z = (N_q - N_{\bar{q}})/x$. Parameter $a = 1 + (\bar{N}_M/\bar{N}_B)_{z=0}/3$ denotes the production competition of baryon

to meson and is tuned to be $a \approx 4.86 \pm 0.1$ according to our recent work [35].

In this paper, we only consider the production of the ground state $J^P = 0^-, 1^-$ mesons and $J^P = (1/2)^+, (3/2)^+$ baryons in flavor SU(3) group. In meson formation, we introduce a parameter $R_{V/P}$ to describe the relative weight of a quark-antiquark pair forming the state of spin 1 to that of spin 0. Here, we take $R_{V/P} = 0.55 \pm 0.05$ to reproduce the measured K^*/K and ϕ/K data in high-energy reactions [37,38]. Factor C_{M_j} is then parameterized as

$$C_{M_j} = \begin{cases} \frac{1}{1+R_{V/P}} & \text{for } J^P = 0^- \text{ mesons,} \\ \frac{R_{V/P}}{1+R_{V/P}} & \text{for } J^P = 1^- \text{ mesons.} \end{cases} \quad (24)$$

In baryon formation, we introduce a parameter $R_{D/O}$ to describe the relative weight of spin 3/2 state to 1/2 state for three quark combination. We take $R_{D/O} = 0.5 \pm 0.04$ by fitting the experimental data of Ξ^*/Ξ and Σ^*/Λ in high-energy collisions [39]. Then we have for C_{B_j}

$$C_{B_j} = \begin{cases} \frac{1}{1+R_{D/O}} & \text{for } J^P = (1/2)^+ \text{ baryons,} \\ \frac{R_{D/O}}{1+R_{D/O}} & \text{for } J^P = (3/2)^+ \text{ baryons,} \end{cases} \quad (25)$$

except that $C_\Lambda = C_{\Sigma^0} = 1/(2 + R_{D/O})$, $C_{\Sigma^*0} = R_{D/O}/(2 + R_{D/O})$, $C_{\Delta^{++}} = C_{\Delta^-} = C_{\Omega^-} = 1$.

Taking $f_{q_i}(p)$ as model inputs, we can calculate $f_h(p)$ and N_h of hadrons directly produced at hadronization. Finally, we take the decay contribution of short-life resonances into account according to experimental measurements, and obtain results of final-state hadrons

$$f_{h_i}^{(\text{final})}(p) = f_{h_i}(p) + \sum_{i \neq j} \int d p' f_{h_i}(p') D_{ij}(p', p), \quad (26)$$

where the decay function $D_{ij}(p', p)$ is determined by the decay kinematics and decay branch ratios [40].

III. STRANGENESS NEUTRALIZATION IN HEAVY-ION COLLISIONS

In relativistic heavy-ion collisions, strange quark and antiquark are always created in pair in collisions and therefore strangeness is globally conserved. However, for a finite kinetic region such as the midrapidity region, the strangeness neutralization is not so explicit, in particular, at low collision energies. In this section, using the precise data for yield densities and p_T spectra of identified hadrons [29,41–46], we study the local strangeness in the midrapidity region in Au+Au collisions at STAR BES energies.

A. Strangeness at midrapidity

In this subsection, we estimate strangeness density $dN_{\bar{s}}/dy - dN_s/dy$ in the midrapidity region in relativistic heavy-ion collisions. We write $N_{\bar{s}} - N_s$ for short in the following. Since experimental measurements are mainly for hadrons in ground state in flavor SU(3), we estimate the strangeness

by yield densities of the following hadrons:

$$\begin{aligned} N_{\bar{s}} - N_s &= (K^+ + K^0 + K^{*+} + K^{*0}) \\ &\quad - (K^- + \bar{K}^0 + K^{*-} + \bar{K}^{*0}) \\ &\quad - (\Lambda + \Sigma^{0,\pm} + \Sigma^{*0,*\pm} + 2\Xi^{-,0} + 2\Xi^{*- ,0} + 3\Omega^-) \\ &\quad + (\bar{\Lambda} + \bar{\Sigma}^{0,\mp} + \bar{\Sigma}^{*0,*\mp} + 2\bar{\Xi}^{+,0} + 2\bar{\Xi}^{*+,0} + 3\bar{\Omega}^+). \end{aligned} \quad (27)$$

For convenience, we use h to denote dN_h/dy . The contribution of baryons with different charge states is also abbreviated, e.g., $\Sigma^{0,\pm} \equiv \Sigma^0 + \Sigma^- + \Sigma^+$. We note that the contribution of higher mass resonances can be effectively included if we identify above ground state hadrons as the measured ones.

The strangeness in meson sector can be calculated as

$$\begin{aligned} K^+ + K^0 + K^{*+} + K^{*0} - K^- - \bar{K}^0 - K^{*-} - \bar{K}^{*0} \\ = (K^+ - K^-)_{\text{final}} + (K^0 - \bar{K}^0)_{\text{final}}, \end{aligned} \quad (28)$$

where we use the subscript “final” to denote that $K^+ - K^-$ and $K^0 - \bar{K}^0$ have received the decay contribution of K^{*} . Since neutral kaons are not measured, we use the approximation

$$(K^+ - K^-)_{\text{final}} \approx (K^0 - \bar{K}^0)_{\text{final}}. \quad (29)$$

For strangeness contained in hyperons with one strange quark, we decompose them into two parts: experimentally measured net- Λ and experimentally un-measured net- Σ^\pm . Using the property of S&EM decays for hyperons [40], we have

$$\begin{aligned} (\Lambda + \Sigma^{0,\pm} + \Sigma^{*0,*\pm}) - (\bar{\Lambda} + \bar{\Sigma}^{0,\mp} + \bar{\Sigma}^{*0,*\mp}) \\ = (\Lambda - \bar{\Lambda})_{\text{final}} + (\Sigma^\pm - \bar{\Sigma}^\mp)_{\text{final}}, \end{aligned} \quad (30)$$

with

$$\begin{aligned} (\Lambda - \bar{\Lambda})_{\text{final}} &= (\Lambda - \bar{\Lambda}) + (\Sigma^0 - \bar{\Sigma}^0) + 0.94(\Sigma^{*\pm} - \bar{\Sigma}^{*\mp}) \\ &\quad + 0.88(\Sigma^{*0} - \bar{\Sigma}^{*0}) \end{aligned} \quad (31)$$

and

$$\begin{aligned} (\Sigma^\pm - \bar{\Sigma}^\mp)_{\text{final}} &= (\Sigma^\pm - \bar{\Sigma}^\mp) + 0.06(\Sigma^{*\pm} - \bar{\Sigma}^{*\mp}) \\ &\quad + 0.12(\Sigma^{*0} - \bar{\Sigma}^{*0}). \end{aligned} \quad (32)$$

Applying our formula of hadronic yields in Sec. II, we obtain

$$\frac{(\Sigma^\pm - \bar{\Sigma}^\mp)_{\text{final}}}{(\Lambda - \bar{\Lambda})_{\text{final}}} = \frac{1.1 + 0.68R_{D/O} + 0.099R_{D/O}^2}{1.096 + 2.62R_{D/O} + R_{D/O}^2} \approx 0.55. \quad (33)$$

For strangeness contained in hyperons with two strange quarks, after considering S&EM decays, we have

$$(\Xi^{-,0} - \bar{\Xi}^{+,0}) + (\Xi^{*- ,0} - \bar{\Xi}^{*+,0}) = (\Xi^{-,0} - \bar{\Xi}^{+,0})_{\text{final}}, \quad (34)$$

and we use the approximation

$$(\Xi^- - \bar{\Xi}^+)_{\text{final}} \approx (\Xi^0 - \bar{\Xi}^0)_{\text{final}}. \quad (35)$$

By the sum over the strangeness in meson and baryon sectors, we obtain the net-strangeness of the system

$$\begin{aligned} N_{\bar{s}} - N_s &\approx 2(K^+ - K^-)_{\text{final}} - 1.57(\Lambda - \bar{\Lambda})_{\text{final}} \\ &\quad - 4(\Xi^- - \bar{\Xi}^+)_{\text{final}} - 3(\Omega^- - \bar{\Omega}^+), \end{aligned} \quad (36)$$

where subscript “final” denotes the yield including S&EM decay contributions.

The total number of strange quarks and strange antiquarks is

$$\begin{aligned} N_{\bar{s}} + N_s &\approx 2(K^+ + K^-)_{\text{final}} + 1.57(\Lambda + \bar{\Lambda})_{\text{final}} \\ &\quad + 4(\Xi^- + \bar{\Xi}^+)_{\text{final}} + 3(\Omega^- + \bar{\Omega}^+) \\ &\quad + 2\phi + 2\left(\frac{2}{3}\eta + \frac{1}{3}\eta'\right). \end{aligned} \quad (37)$$

Because the strangeness $N_{\bar{s}} - N_s$ is explicitly dependent on collision energies and collision centralities, we define the relative asymmetry factor

$$z_S = \frac{N_{\bar{s}} - N_s}{N_{\bar{s}} + N_s}, \quad (38)$$

which is convenient to compare results in different situations.

In Table I, we show results for z_S in most central Au+Au collisions at different collision energies.¹ Experimental data for yield densities of hadrons that are used in calculation are also presented ([41–45], [29,47]). Because some data for Ω^- and ϕ are results in 0–10% centrality, we rescale them by multiplying a factor $N_{\text{part}}^{(0-5\%)} / N_{\text{part}}^{(0-10\%)}$ according to the participant nucleon number N_{part} . We do the similar rescaling for data of Ω^- in 0–60% centrality at $\sqrt{s_{NN}} = 7.7$ GeV. Because data of η and η' mesons are usually absent, we neglect them and therefore the calculated z_S is overestimated. We see that z_S at seven collision energies are quite small. Therefore, strangeness neutralization $N_s = N_{\bar{s}}$ is well satisfied in midrapidity region in heavy-ion collisions at RHIC energies.

B. p_T spectrum symmetry

In this subsection, we study the symmetry property between p_T spectrum of strange quark $f_s(p_T)$ and that of strange antiquark $f_{\bar{s}}(p_T)$. For this purpose, we choose Ω^- ($\bar{\Omega}^+$) which consists of only strange quarks (antiquarks). Using Eq. (7), we have

$$f_{\Omega}(3p_T) = \kappa_{\Omega} f_s^3(p_T), \quad (39)$$

$$f_{\bar{\Omega}}(3p_T) = \kappa_{\bar{\Omega}} f_{\bar{s}}^3(p_T), \quad (40)$$

from which we have

$$\frac{f_{\bar{s}}(p_T)}{f_s(p_T)} = \kappa_{\bar{\Omega},\Omega} \left[\frac{f_{\bar{\Omega}}(3p_T)}{f_{\Omega}(3p_T)} \right]^{1/3} \propto \left[\frac{f_{\bar{\Omega}}(3p_T)}{f_{\Omega}(3p_T)} \right]^{1/3}, \quad (41)$$

¹In calculations, we use the approximation of isospin symmetry between up and down quarks in Eqs. (29) and (35). If we consider the small asymmetry in number between up quarks and down quarks coming from colliding nucleons, then we should modify Eq. (29) by multiplying a factor N_u/N_d and Eq. (35) by multiplying a factor $(N_u/N_d)^{-1}$ in right-hand side of the equation and the corresponding coefficients in Eqs. (36) and (37). According to the number of newborn quarks extracted in next section and net-quarks from participant nucleons, we obtain, for example, $N_u/N_d \approx 0.99$ at $\sqrt{s_{NN}} = 200$ GeV and $N_u/N_d \approx 0.93$ at 7.7 GeV. The resulting z_S are $(-0.004, -0.018, -0.0014, -0.005, 0.002, 0.003, -0.009)$ at $\sqrt{s_{NN}} = (200, 62.4, 39, 27, 19.6, 11.5, 7.7)$ GeV, respectively. They are very close to those shown in Table I.

TABLE I. Strangeness asymmetry factor z_S calculated by yield data of strange hadrons and antihadrons in central Au+Au collisions [29,41–45,47].

$\sqrt{s_{NN}}$ (GeV)	$K^{+,-}$	$\Lambda(\bar{\Lambda})$	$\Xi^-(\bar{\Xi}^+)$	$\Omega^-(\bar{\Omega}^+)$	ϕ	z_S
200	48.9 ± 6.3	16.7 ± 1.1	2.17 ± 0.2	0.53 ± 0.06	7.95 ± 0.11	-0.004 ± 0.06
	45.7 ± 5.2	12.7 ± 0.9	1.83 ± 0.2			
62.4	37.6 ± 2.7	15.7 ± 2.3	1.63 ± 0.2	0.212 ± 0.028	3.52 ± 0.08	-0.019 ± 0.04
	32.4 ± 2.3	8.3 ± 1.1	1.03 ± 0.11	0.167 ± 0.027		
39	32.0 ± 2.9	11.02 ± 0.03	1.54 ± 0.01	0.191 ± 0.006	3.38 ± 0.03	-0.002 ± 0.05
	25.0 ± 2.3	3.82 ± 0.01	0.78 ± 0.01	0.139 ± 0.004		
27	31.1 ± 2.8	11.67 ± 0.04	1.57 ± 0.01	0.154 ± 0.008	3.01 ± 0.04	-0.006 ± 0.05
	22.6 ± 2.0	2.75 ± 0.01	0.598 ± 0.006	0.0972 ± 0.0049		
19.6	29.6 ± 2.9	12.58 ± 0.04	1.62 ± 0.02	0.155 ± 0.01	2.57 ± 0.04	-0.0002 ± 0.05
	18.8 ± 1.9	1.858 ± 0.009	0.421 ± 0.005	0.0811 ± 0.0048		
11.5	25.0 ± 2.5	14.17 ± 0.08	1.35 ± 0.02	0.082 ± 0.012	1.72 ± 0.04	-0.004 ± 0.05
	12.3 ± 1.2	0.659 ± 0.009	0.169 ± 0.004	0.0356 ± 0.0052		
7.7	20.8 ± 1.7	15.3 ± 0.11	1.19 ± 0.03	0.0271 ± 0.0048	1.21 ± 0.06	-0.021 ± 0.04
	7.7 ± 0.6	0.193 ± 0.006	0.0667 ± 0.0044	0.0075 ± 0.0013		

where $\kappa_{\bar{\Omega},\Omega} = (\kappa_{\bar{\Omega}}/\kappa_{\Omega})^{1/3}$ is independent of p_T but is dependent on quark numbers. We emphasize that $\kappa_{\bar{\Omega},\Omega}$ is not equal to one at nonzero net quark number.

Using data of p_T spectra for Ω^- and $\bar{\Omega}^+$ in central Au+Au collisions [29,47], we calculate the ratio $f_{\bar{s}}(p_T)/f_s(p_T)$ at different collision energies and present results in Fig. 1. Since we have shown $N_s = N_{\bar{s}}$ in the previous subsection, we multiply a proper constant before data of $f_{\bar{\Omega}}^{1/3}(3p_T)/f_{\Omega}^{1/3}(3p_T)$ to satisfy $N_s = N_{\bar{s}}$ and therefore we can directly compare $f_{\bar{s}}(p_T)/f_s(p_T)$ in/at different collision centralities/energies. Because of finite statistics of Ω^- and $\bar{\Omega}^+$, data points of $f_{\bar{s}}(p_T)/f_s(p_T)$ show a certain fluctuations around one. On the whole, we can see that $f_{\bar{s}}(p_T) = f_s(p_T)$ is a good approximation at the studied collision energies.

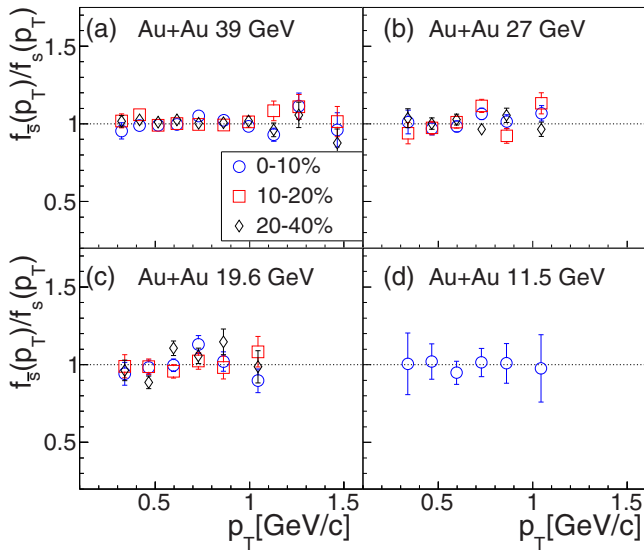


FIG. 1. Ratio $f_{\bar{s}}(p_T)/f_s(p_T)$ in Au+Au collisions at different collision energies obtained from experimental data of Ω^- and $\bar{\Omega}^+$ in central and semi-central collisions [29,47] by Eq. (41).

IV. p_T SPECTRA OF HADRONS

In this section, we use the quark combination model (QCM) in Sec. II to study p_T spectra of light-flavor hadrons in Au+Au collisions at RHIC energies. The inputs of model are p_T spectra of quarks and antiquarks at hadronization. Here, we take $f_{\bar{s}}(p_T) = f_s(p_T)$ based on the study of strangeness neutralization in Sec. III. We take $f_{\bar{u}}(p_T) = f_{\bar{d}}(p_T)$ for the newborn up and down antiquarks. Because a part of up and down quarks comes from the colliding nucleons, p_T spectrum of up quarks is not exactly the same as that of down quarks. As discussed in Ref. [47], the relative difference in number between up and down quarks is only a few percentages. We have checked that p_T spectra of hadrons and yield ratios of antihadron to hadron studied in this paper are not sensitive to this small asymmetry. Therefore, in this paper, we take the approximation $f_u(p_T) \approx f_d(p_T)$ in the midrapidity region.

In Table II, we list all inputs and parameters of the model which are needed to calculate p_T spectra of hadrons. As introduced in model description in Sec. II, two parameters $R_{V/P}$ and $R_{D/O}$ are taken as 0.55 and 0.5, respectively, at all the studied collision energies. For three inputs, $f_s(p_T)$ is fixed by using our model to fit experimental data of ϕ , and $f_u(p_T)$ ($f_{\bar{u}}(p_T)$) is fixed by experimental data of (anti)baryons containing $u(\bar{u})$ such as (anti)proton [44,46,47], respectively. The extracted results for quark p_T spectra in Au+Au collisions for 0-5% centrality at six RHIC energies are shown in Fig. 2.

In Fig. 3, we show the calculated results for p_T spectra of hadrons in central Au+Au collisions at $\sqrt{s_{NN}} = 200$ GeV and compare them with experimental data [21,42,43]. We see that the agreement between our model results and

TABLE II. Inputs and parameters of the model to calculation p_T spectra of hadrons.

Input		Parameter		
$f_u(p_T)$	$f_{\bar{u}}(p_T)$	$f_s(p_T)$	$R_{V/P}$	$R_{D/O}$

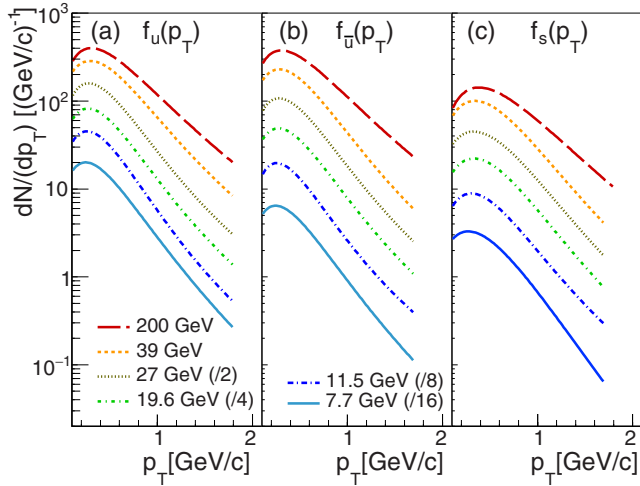


FIG. 2. p_T spectra of quarks at hadronization at midrapidity in Au+Au collisions for 0–5% centrality. Spectra at $\sqrt{s_{NN}} = 7.7$ –27 GeV are scaled for clarity as shown in the figure.

experimental data is satisfactory. Although there exists many successful explanations on these experimental data in the framework of quark combination mechanism in previous works [9,10,13,14,34,48], here we would like to emphasize that the current EVC model can systematically explain these data in a simple way. Furthermore, the good agreement at top RHIC energy provides important basis for the application of our model to lower RHIC energies.

In Figs. 4–8, we show results for p_T spectra of hadrons in central Au+Au collisions at $\sqrt{s_{NN}} = 39, 27, 19.6, 11.5$, and 7.7 GeV and compare with experimental data [29,46,47].

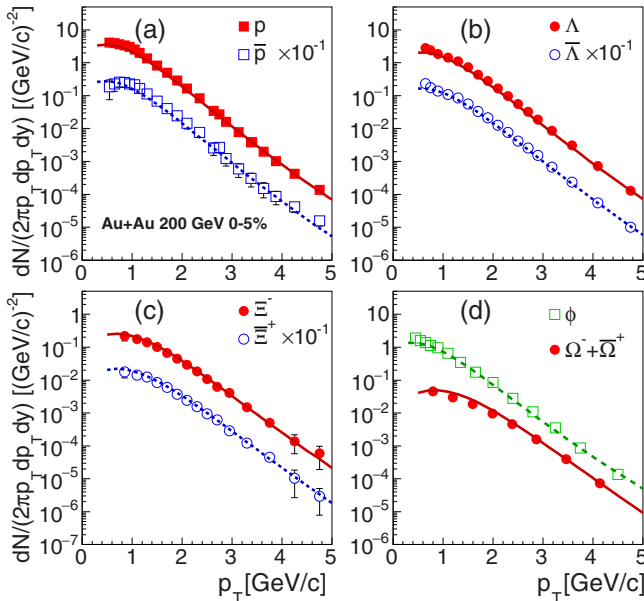


FIG. 3. p_T spectra of hadrons at midrapidity in central Au+Au collisions at $\sqrt{s_{NN}} = 200$ GeV. Symbols are experimental data [21,42,43] and lines are results of our model. Spectra of some hadrons are scaled for clarity as shown in the figure.

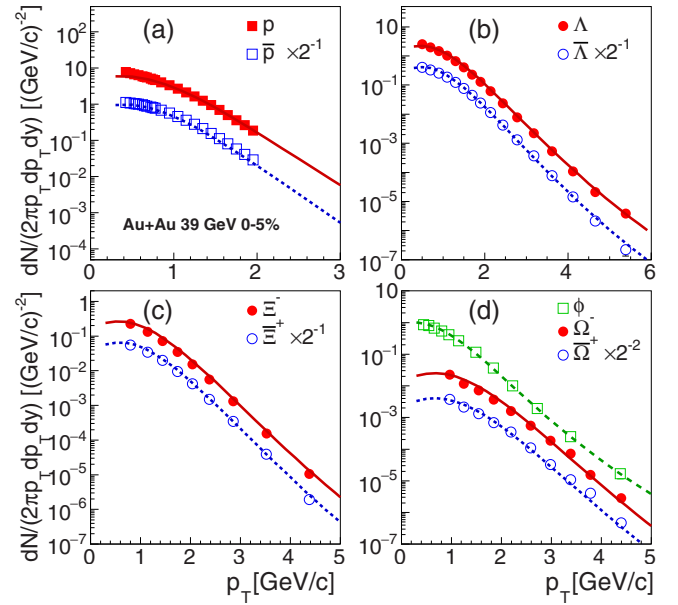


FIG. 4. Same as described in the caption of Fig. 3 but for central Au+Au collisions at $\sqrt{s_{NN}} = 39$ GeV. Experimental data are from Refs. [29,46,47].

At $\sqrt{s_{NN}} = 39, 27, 19.6, 11.5$ GeV, we see a good agreement between our model results and experimental data [29,46,47]. In particular, we see that experimental data for baryons (p, Λ, Ξ, Ω) and meson ϕ can be explained by the model very well. At $\sqrt{s_{NN}} = 7.7$ GeV, we also see that model results are in good agreement with available experimental data. However, compared with data in Figs. , the available data at $\sqrt{s_{NN}} = 7.7$ GeV cover smaller p_T range and Ω data in the most central

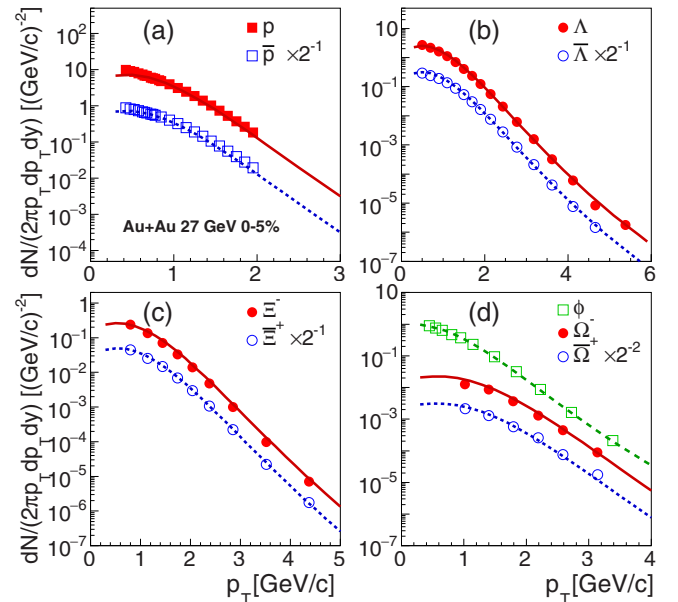


FIG. 5. Same as described in the caption of Fig. 3 but for central Au+Au collisions at $\sqrt{s_{NN}} = 27$ GeV. Experimental data are from Refs. [29,46,47].

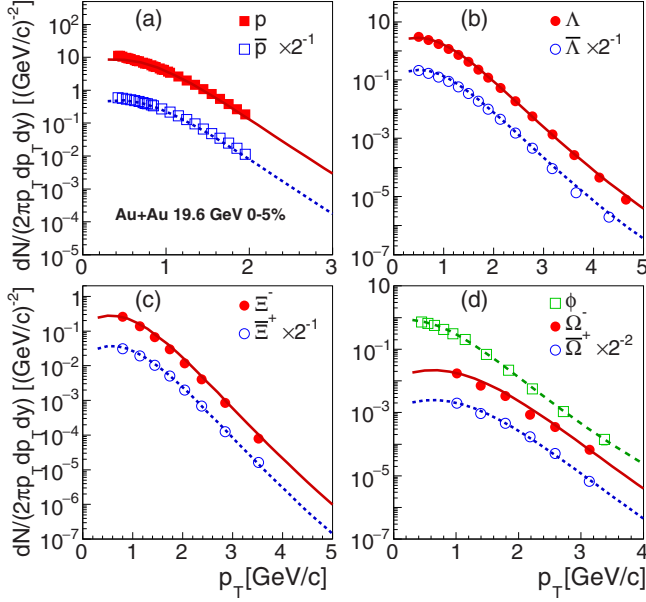


FIG. 6. Same as described in the caption of Fig. 3 but for central Au+Au collisions at $\sqrt{s_{NN}} = 19.6$ GeV. Experimental data are from Refs. [29,46,47].

collisions are absent. Therefore the comparison at $\sqrt{s_{NN}} = 7.7$ GeV is not as conclusive as those at other five higher energies. We should study this energy point further in the future when more precise data are available.

Using these systematic calculations and comparisons, we would like to emphasize the equal-velocity combination of quarks and antiquarks as the effective description at hadronization. This is manifested by the following two points.

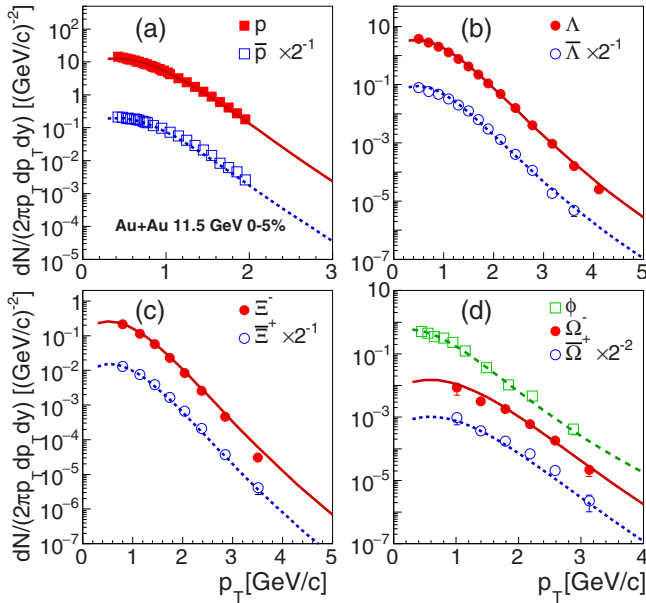


FIG. 7. Same as described in the caption of Fig. 3 but for central Au+Au collisions at $\sqrt{s_{NN}} = 11.5$ GeV. Experimental data are from Refs. [29,46,47].

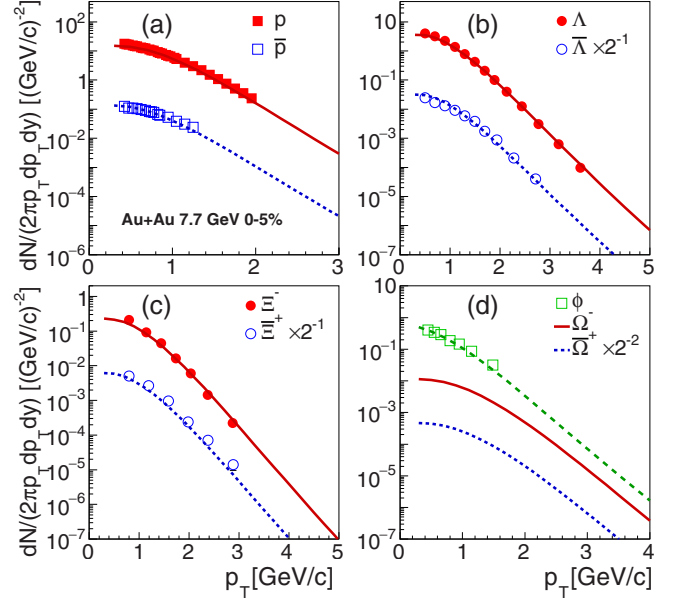


FIG. 8. Same as described in the caption of Fig. 3 but for central Au+Au collisions at $\sqrt{s_{NN}} = 7.7$ GeV. Experimental data are from Refs. [29,46,47].

First, from panel (d) in Figs. 3–7, we see that experimental data of Ω and ϕ can be perfectly explained by the same $f_s(p_T)$ in a very simple way,

$$f_{\Omega}(p_T) = \kappa_{\Omega} f_s^3(p_T/3), \quad (42)$$

$$f_{\phi}(p_T) = \kappa_{\phi} f_s^2(p_T/2). \quad (43)$$

We call this property as the quark number scaling for hadronic p_T spectra. We have shown that this property not only exists in relativistic heavy-ion collisions but also exists in high-multiplicity pp and p -Pb collisions at LHC energies [23,24,28]. Second, we see that data of Λ and Ξ^- can be simultaneously explained by $f_s(p_T)$ from ϕ and $f_u(p_T)$ from proton,

$$f_{\Lambda}(p_T) = \kappa_{\Lambda} f_u^2\left(\frac{1}{2+r}p_T\right) f_s\left(\frac{r}{2+r}p_T\right), \quad (44)$$

$$f_{\Xi}(p_T) = \kappa_{\Xi} f_u\left(\frac{1}{1+2r}p_T\right) f_s^2\left(\frac{r}{1+2r}p_T\right), \quad (45)$$

after further including the decay contribution of heavier baryons. Here, $r = m_s/m_u$. This is a clear support for the equal-velocity combination for quarks with different flavors.

V. HADRONIC YIELDS AND MULTIPARTICLE CORRELATIONS

In this section, we study the p_T -integrated yields of identified hadrons. In heavy-ion collisions at RHIC energies, the net baryon numbers deposited in the midrapidity region will influence the production of hadrons and antihadrons to a certain extent. One of the consequences for nonzero baryon number density is the asymmetry in yield between hadrons and their

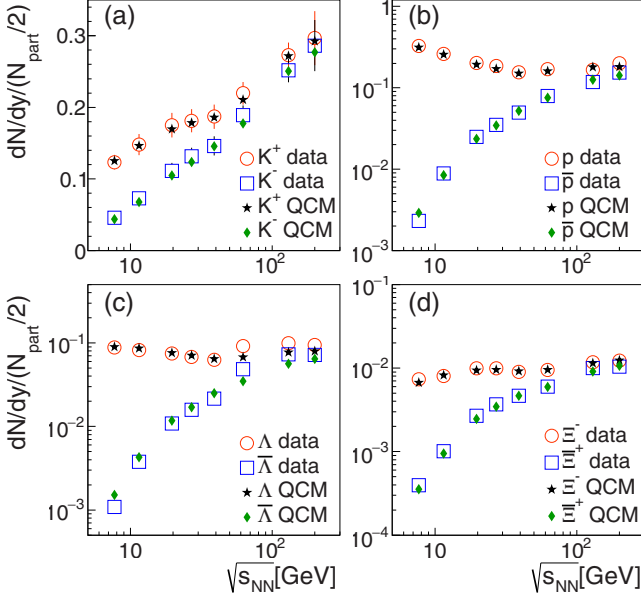


FIG. 9. Hadronic yield densities divided by participant nucleon number at midrapidity in Au+Au collisions at different collision energies. Open symbols are experimental data [29,42,44–46,49,50] and solid symbols are model results.

antiparticles. We study this yield asymmetry with our model by focusing on multiparticle yield correlations.

In Fig. 9, we show yield densities of hadrons and antihadrons² divided by participant nucleon number at midrapidity in central Au+Au collisions at different collision energies. Open symbols are experimental data [29,42,44–46,49,50] and solid symbols are model results. Experimental data show that the yield split between K^+ and K^- in (a) is much smaller than that between p and \bar{p} in (b). Yield split between Λ and $\bar{\Lambda}$ in (c) and that between Ξ^- and Ξ^+ in (d) are larger than kaon split in (a) but are smaller than proton split in (b). Comparing with experimental data, we see that the model provides a globally good description for yield densities of hadrons and antihadrons.

To further study the split in yield between hadrons and antihadrons, we calculate the ratio of yield for antihadron to that for hadron. Yield ratio is not sensitive to the numbers of quarks and antiquarks at hadronization and is also not sensitive to some hadronization details such as parameters $R_{V/P}$ and $R_{D/O}$ introduced in our model. Therefore, it can be used to provide a more direct test for the quark combination mechanism at hadronization in relativistic heavy-ion collisions. Experimentally measured protons and antiprotons contain complex decay contributions of heavier baryons and

antibaryons,

$$p^{(\text{final})} = p + \Delta^{++} + \frac{2}{3}\Delta^+ + \frac{1}{3}\Delta^0 + 0.64\Lambda + 0.517\Sigma^+ + 0.64\Sigma^0 + 0.633\Sigma^{*+} + 0.594\Sigma^{*0} + 0.602\Sigma^{*-} + 0.64(\Xi^0 + \Xi^- + \Xi^{*0} + \Xi^{*-}) + 0.64\Omega^-, \quad (46)$$

where we use the particle name with superscript “(final)” to denote the yield density of final-state hadron receiving the decay contributions and the particle name without superscript in the right-hand side of the equation to denote yields of directly-produced hadrons by hadronization. The ratio \bar{p}/p finally behaves as

$$\frac{\bar{p}^{(\text{final})}}{p^{(\text{final})}} \approx \left(\frac{1-z}{1+z} \right)^{0.99a}, \quad (47)$$

where z is net-quark fraction and the factor $a \approx 4.86$ is related to the baryon-meson production competition [35,36], see Eq. (23) and texts below. For yields of kaons, we take the decay contributions of $K^*(892)$ and ϕ into account and have

$$\begin{aligned} \frac{K^{-(\text{final})}}{K^{+(\text{final})}} &= \frac{K^- + \frac{1}{3}K^{*-} + \frac{2}{3}K^{*0} + 0.489\phi}{K^+ + \frac{1}{3}K^{*+} + \frac{2}{3}K^{*0} + 0.489\phi} \\ &= \frac{1-z}{1+z} \frac{1 + 0.489C_\phi\lambda_s}{1 + \lambda_s \left(\frac{z}{1+z} + 0.489C_\phi \frac{1-z}{1+z} \right)}, \end{aligned} \quad (48)$$

where $\lambda_s = N_s/N_{\bar{u}}$.

For yields of Λ , Ξ^- and their antiparticles, we consider the S&EM decay contributions,

$$\begin{aligned} \frac{\bar{\Lambda}^{(\text{final})}}{\Lambda^{(\text{final})}} &= \frac{\bar{\Lambda} + \bar{\Sigma}^0 + 0.94(\bar{\Sigma}^{*-} + \bar{\Sigma}^{*+}) + 0.88\bar{\Sigma}^{*0}}{\Lambda + \Sigma^0 + 0.94(\Sigma^{*+} + \Sigma^{*-}) + 0.88\Sigma^{*0}} \\ &= \left(\frac{1-z}{1+z} \right)^{a-1} \left(1 + \lambda_s \frac{z}{1+z} \right)^{-2}, \end{aligned} \quad (49)$$

and

$$\begin{aligned} \frac{\bar{\Xi}^{+(\text{final})}}{\Xi^{-(\text{final})}} &= \frac{\bar{\Xi}^+ + \frac{1}{3}\bar{\Xi}^{*+} + \frac{2}{3}\bar{\Xi}^{*0}}{\Xi^- + \frac{1}{3}\Xi^{*-} + \frac{2}{3}\Xi^{*0}} \\ &= \left(\frac{1-z}{1+z} \right)^{a-2} \left(1 + \lambda_s \frac{z}{1+z} \right)^{-1}. \end{aligned} \quad (50)$$

For Ω^- , we directly have

$$\frac{\bar{\Omega}^+}{\Omega^-} = \left(\frac{1-z}{1+z} \right)^{a-3}. \quad (51)$$

In Eqs. (48)–(50), the power term $[(1-z)/(1+z)]^a$ dominates the behavior of three ratios. Therefore, ratios K^-/K^+ , \bar{p}/p , $\bar{\Lambda}/\Lambda$, $\bar{\Xi}^+/\Xi^-$, and $\bar{\Omega}^+/\Omega^-$ in our model are simply correlated with each other by the net-quark fraction z .

²Model results for yield densities of kaons are presented here. Because the direct combination $u + \bar{s} \rightarrow K$ in the current EVC model has energy conservation issue, we have to introduce further treatment to reconcile this such as we did in Ref. [25]. However, the strange quantum number conservation ensures that the number of the formed kaon can be correctly calculated in the current model.

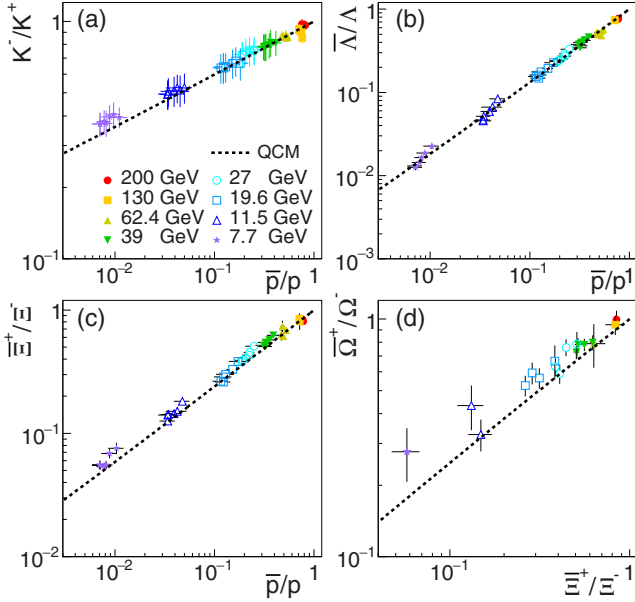


FIG. 10. antihadron to hadron yield ratios in Au+Au collisions at different collision energies. Symbols are experimental data in central and semi-central (centrality <60%) collisions [29,42,44–46,49–51]. Dashed lines are model results.

Based on Eqs. (47)–(51), we can build several multihadron correlations as more sensitive tests of quark combination mechanism. In Fig. 10(a), we first show the correlation between K^-/K^+ and \bar{p}/p . This correlation shows how the production of baryon and that of meson in heavy-ion collisions are simultaneously influenced by the baryon quantum number density characterized by net-quark fraction z in our model. Symbols are experimental data at midrapidity in central and semicentral collisions [29,42,44–46,49–51]. Error bars are the quadratic sum of statistical and systematic uncertainties. The dashed line is the result of QCM by Eqs. (47) and (48). Different from our previous work [36] and previous experimental measurements [51], here we show the correlation in double-logarithmic coordinates to provide a full and clear presentation because ratio \bar{p}/p changes much faster than K^-/K^+ . We see that experimental data in double-logarithmic coordinates behave as almost a straight line and our model can well reproduce this correlation.

In Fig. 10(b) we show the correlation between $\bar{\Lambda}/\Lambda$ and \bar{p}/p . We see that experimental data, symbols in the figure, exhibit a linear behavior in double-logarithmic coordinates. This behavior can be perfectly reproduced in our model by Eqs. (47) and (49); see the dashed line. In addition, we note that ratio $\bar{\Lambda}/\Lambda$ decreases slower than \bar{p}/p by a factor $(1-z)/(1+z) = N_{\bar{q}}/N_q$. This is because that, compared with \bar{p}/p , ratio $\bar{\Lambda}/\Lambda$ involves a strangeness neutralization $N_{\bar{s}}/N_s = 1$.

In Fig. 10(c) we show the correlation between $\bar{\Xi}^+/\Xi^-$ and \bar{p}/p . Experimental data also exhibit a linear behavior in double-logarithmic coordinates. Since $\bar{\Xi}^+/\Xi^-$ involves double effect of strangeness neutralization $(N_{\bar{s}}/N_s)^2 = 1$, $\bar{\Xi}^+/\Xi^-$ decreases slower than $\bar{\Lambda}/\Lambda$ as the function of \bar{p}/p . Our model result Eqs. (47) and (50), the dashed line in the figure, can

well describe data at $\sqrt{s_{NN}} \geq 11.5$ GeV and slightly underestimates $\bar{\Xi}^+/\Xi^-$ at $\sqrt{s_{NN}} = 7.7$ GeV.

In Fig. 10(d), we further show the correlation among multistrangeness hadrons $\bar{\Omega}^+/\Omega^-$ and $\bar{\Xi}^+/\Xi^-$. Experimental data in double-logarithmic coordinates also exhibit a linear behavior. Because Ω^- ($\bar{\Omega}^+$) completely consists of strange (anti)quarks, ratio $\bar{\Omega}^+/\Omega^-$ involves triple effect of strangeness neutralization and therefore it decreases slower than $\bar{\Xi}^+/\Xi^-$. The model result by Eqs. (50) and (51), the dashed line in the figure, can roughly describe data at $\sqrt{s_{NN}} \geq 11.5$ GeV and underestimates $\bar{\Omega}^+/\Omega^-$ at $\sqrt{s_{NN}} = 7.7$ GeV to a certain extent.

Some discussions on the above results are necessary. First, we emphasize the key physics in our model relating to multihadron correlations shown in Fig. 10. As shown by Eqs. (47)–(51), correlations among yield ratios of antihadron to hadron are not sensitive to absolute numbers of quarks and antiquarks at hadronization and nonperturbative parameters $R_{V/P}$ and $R_{D/O}$ introduced in the model. Therefore, these yield correlations are only related to two basic features of quark combination in our model. (1) free combination. Newborn quarks and antiquarks, net-quarks are all treated as individual (anti)quarks and freely take part in combination. (2) flavor independent combination probability. We take \bar{N}_B/N_q^3 as the averaged probability of $q_1q_2q_3$ forming a baryon and $\bar{N}_M/(N_qN_{\bar{q}})$ as the averaged probability of $q_1\bar{q}_2$ forming a meson. No sophisticated flavor correction is made at the moment. From Fig. 10, we see that such a global quark combination model provides a systematic description on multihadron yield correlations in Au+Au collisions, at least at $\sqrt{s_{NN}} \geq 11.5$ GeV. Therefore, this is a clear signal of quark combination mechanism at hadronization in these collisions.

Second, the comparison between our model calculation and experimental data in Au+Au collisions at $\sqrt{s_{NN}} = 7.7$ GeV may indicate some physics beyond the key features of quark combination discussed above. As \bar{p}/p and $\bar{\Lambda}/\Lambda$ ratios are reproduced, we see that model results for K^-/K^+ , $\bar{\Xi}^+/\Xi^-$, and $\bar{\Omega}^+/\Omega^-$ are smaller than experimental data to a certain extent. This may be related to the point (1) discussed above. In Au+Au collisions at low energy, the colliding nucleons may not break completely. A part of nucleon fragments may do not behave as the individual up/down quarks and freely take part in the combination with newborn quarks and antiquarks; instead, they behave as diquarks and can form proton by combining with a up/down quark or form Λ by combining with a strange quark. Because these net-quarks only contribute to proton and Λ production, net-quark fraction z used in Eqs. (48), (50), and (51) for K^-/K^+ , $\bar{\Xi}^+/\Xi^-$, and $\bar{\Omega}^+/\Omega^-$ should be smaller than that in \bar{p}/p and $\bar{\Lambda}/\Lambda$. This consideration can increase ratios K^-/K^+ , $\bar{\Xi}^+/\Xi^-$, and $\bar{\Omega}^+/\Omega^-$ at the given \bar{p}/p and $\bar{\Lambda}/\Lambda$ ratios and therefore can qualitatively improve the description at $\sqrt{s_{NN}} = 7.7$ GeV in the current model. Such a sophisticated effect of net-quarks is worthwhile to be studied in detail in the future works.

VI. PROPERTIES OF QUARK DISTRIBUTIONS

By studying experimental data of hadronic p_T spectra, we have obtained p_T spectra of quarks at hadronization, which

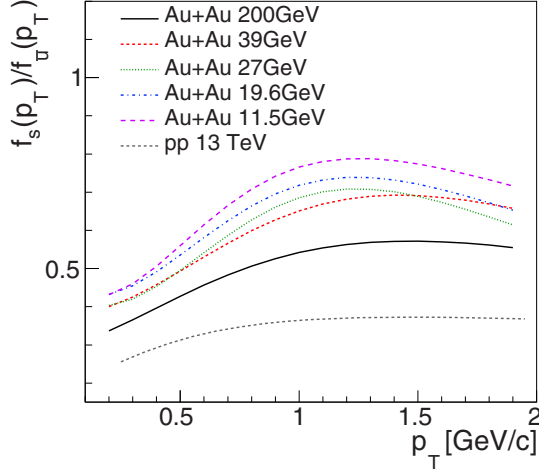


FIG. 11. Spectrum ratio $f_s(p_T)/f_u(p_T)$ in central Au+Au collisions at $\sqrt{s_{NN}} = 200, 39, 27, 19.6,$ and 11.5 GeV, and that in pp collisions at $\sqrt{s} = 13$ TeV.

are shown in Fig. 2. In this section, we study properties of these obtained quark distributions at hadronization.

We first calculate the ratio $f_s(p_T)/f_u(p_T)$ and study its p_T dependence. Fig. 11 shows results in central Au+Au collisions at $\sqrt{s_{NN}} = 200, 39, 27, 19.6,$ and 11.5 GeV. Result of $f_s(p_T)/f_u(p_T)$ in pp collisions at $\sqrt{s} = 13$ TeV [24] is also presented. We see that ratios in Au+Au collisions are obviously higher than that in pp collisions. This means that the production of strange quarks in the studied p_T range in Au+Au collisions is significantly enhanced. In addition, we see that ratios in Au+Au collisions at these collision energies in the low p_T range ($p_T \lesssim 1.3$ GeV/c) all increase with p_T . It is similar to pp results. This property is related to the complex (non)perturbative QCD evolution in connection with quark masses in partonic phase.

We note that the increase of the ratio at low p_T in heavy-ion collisions can be qualitatively understood by thermal statistics. In the case of thermal equilibrium such as the Boltzmann distribution $dN/(p_T dp_T) \propto \exp(-\sqrt{p_T^2 + m^2}/T)$ in two-dimensional transverse momentum space, heavier mass will lead to flatter shape of the p_T distribution and thus lead to the increase of the ratio. However, Boltzmann distribution at hadronization temperature in the rest frame can not directly describe the obtained quark distributions in Fig. 2. We should further take into account the contribution of the collective radial flow in the prior partonic phase evolution in heavy-ion collisions. As an illustration, we consider a simple situation, that is, Boltzmann distribution in the two-dimensional transverse momentum space boosted with a radial flow velocity v_\perp . In this case, the distribution is

$$\frac{dN}{p_T dp_T} \propto \frac{1}{E} E^*(v_\perp) \exp[-E^*(v_\perp)/T], \quad (52)$$

with $E^*(v_\perp) = \gamma_\perp(E - v_\perp p_T)$ and $E = \sqrt{p_T^2 + m^2}$. If we assume that quarks of different flavors at hadronization are thermalized and boosted with the same radial velocity, then we can use the above formula to simultaneously describe

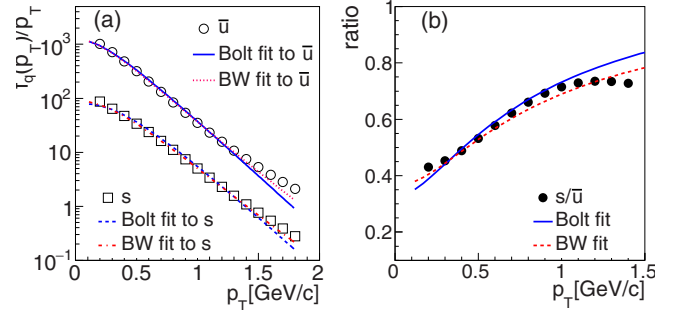


FIG. 12. (a) Fit results for quark p_T spectra at hadronization in central Au+Au collisions at $\sqrt{s_{NN}} = 19.6$ GeV by Boltzmann formula Eq. (52) and by blast-wave model at the same hadronization temperature 0.161 GeV and radial flow velocity $0.25 c$. (b) ratio $f_s(p_T)/f_u(p_T)$ by two fit methods. Symbols are quark p_T spectra and lines are fit results.

the extracted $f_u(p_T)$ and $f_s(p_T)$ in the low p_T range ($p_T \leq 1.3$ GeV/c) in Fig. 2. According to our previous work [28], the hadronization temperature is taken as $T = (0.164, 0.163, 0.162, 0.161, 0.156)$ GeV in central Au+Au collisions at $\sqrt{s_{NN}} = (200, 39, 27, 19.6, 11.5)$ GeV, respectively. We obtain radial flow velocity $v_\perp/c \approx (0.39, 0.28, 0.27, 0.25, 0.23)$ at these collision energies.

We find that these results for radial flow velocity are consistent with our previous extraction by a hydrodynamics-motivated blast-wave model [52] fit of $f_s(p_T)$ with the same hadronization temperature [28]. We also find that $f_u(p_T)$ and $f_s(p_T)$ extracted in this work can also be consistently described in blast-wave mode. Here, taking central Au+Au collisions at $\sqrt{s_{NN}} = 19.6$ GeV as an example, we show in Fig. 12(a) the fit results of quark p_T spectra by Eq. (52) and those by blast-wave model at the same hadronization temperature 0.161 GeV and radial flow velocity $0.25 c$. We see that two fit methods give the consistent description on quark p_T spectra. In addition, we see from Fig. 12(b) that the increase part of the ratio $f_s(p_T)/f_u(p_T)$ in the low p_T range can be reasonably described.

Figure 11 also shows the ratio $f_s(p_T)/f_u(p_T)$ globally increases with the decrease of collision energies. To study this energy dependence of strangeness, we calculate the strangeness factor

$$\lambda_s = \frac{N_s}{N_u} \quad (53)$$

and present results in Fig. 13. Here, results of λ_s in central Au+Au collisions at $\sqrt{s_{NN}} = 62.4$ and 130 GeV are also shown. The uncertainty of λ_s is caused by that of experimental data for yield ratios such as $K/\pi, \Lambda/p, \bar{\Lambda}/\bar{p}$. We note that these new results of λ_s are consistent with our previous works [48,53,54]. Compared with $\lambda_s \approx 0.3$ in elementary collisions such as e^+e^- and pp reactions, we see that $\lambda_s \gtrsim 0.42$ in heavy-ion collisions is obviously enhanced. We also see that λ_s increases as the decrease of collision energy.

The dependence of λ_s on collision energy is related to the varied baryon quantum number density. In this paper, we study this energy dependence in the framework of thermo-

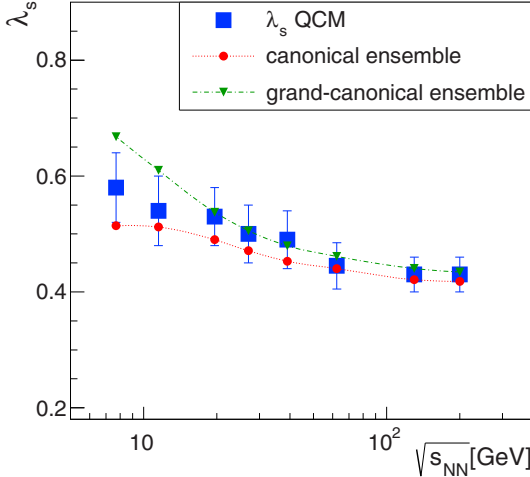


FIG. 13. Strangeness factor $\lambda_s = N_s/N_{\bar{s}}$ in central Au+Au collisions at different collision energies.

dynamics for quark system. We consider a thermal system consisting of constituent quarks and antiquarks. In our quark combination model, constituent quarks and antiquarks are regarded as the effective degrees of freedom at hadronization and they freely combine into baryons and/or mesons at hadronization. Therefore, we can treat such a constituent quark system as the classical gas.

Because we study the production of hadrons in midrapidity range, we first discuss the case of grand-canonical ensemble. The number of quark under Fermi-Dirac statistics in the grand-canonical ensemble is

$$N_f = g \int \frac{d^3x d^3p}{(2\pi)^3} \frac{1}{\exp[(E - \mu_f)/T] + 1} \\ = g \frac{Vm^2T}{2\pi^2} \sum_{n=1}^{\infty} \frac{(-1)^{n+1}}{n} K_2\left(n \frac{m}{T}\right) \exp\left(n \frac{\mu_f}{T}\right), \quad (54)$$

where V is system volume and T is temperature. $g = 6$ is degeneracy factor of quark, m is quark mass and μ_f is chemical potential of quark f . K_2 is the modified Bessel function of the second kind. As discussions of local strangeness conservation in Sec. III, we set $\mu_s = \mu_{\bar{s}} = 0$ to get $N_s = N_{\bar{s}}$. We assume the isospin symmetry between up and down quarks, then we have $\mu_u = \mu_d = -\mu_{\bar{u}} = -\mu_{\bar{d}} = \mu_B/3$. Then, the strangeness factor in grand-canonical ensemble (GCE) of free quark gas is

$$\lambda_s^{(\text{GCE})} = \frac{m_s^2 \sum_{n=1}^{\infty} \frac{(-1)^{n+1}}{n} K_2\left(n \frac{m_s}{T}\right)}{m_u^2 \sum_{n=1}^{\infty} \frac{(-1)^{n+1}}{n} K_2\left(n \frac{m_u}{T}\right) \exp\left[-n \frac{\mu_B}{3T}\right]} \\ \approx \lambda_{s, \mu_B=0}^{(\text{GCE})} \exp\left[\frac{\mu_B}{3T}\right]. \quad (55)$$

In the second line, we consider only the leading term $n = 1$, which is corresponding to the Boltzmann statistics. As we know, baryon chemical potential is increased as the decrease of the collision energy. Therefore, the collision energy dependence of λ_s is qualitatively understood.

For a demonstrative calculation for the collision energy dependence of $\lambda_s^{(\text{GCE})}$, we first apply Eq. (55) with the re-

tuned $m_u = 0.3$ GeV and $m_s = 0.54$ GeV to give a proper strangeness at vanishing baryon chemical potential $\lambda_{s, \mu_B=0}^{(\text{GCE})} \approx 0.42$. Then, we apply Eq. (54) to fit the total quark number $x = N_q + N_{\bar{q}}$ and net-quark number $xz = N_q - N_{\bar{q}}$ integrated from Fig. 2 and obtain V and μ_B of quark system at hadronization. Here, the hadronization temperature is taken as before. Then we substitute μ_B and T into Eq. (55). The calculated results for $\lambda_s^{(\text{GCE})}$ at RHIC energies are shown as triangles with the dashed line in Fig. 13. We see that the extracted λ_s in quark combination model can be explained by grand-canonical ensemble of quark gas system at $\sqrt{s_{NN}} \gtrsim 20$ GeV. At lower two collision energies, GCE results are higher than our extraction.

Considering the longitudinal rapidity space of heavy-ion collisions is finite, in particular, $y_{\text{beam}} < 2.5$ at $\sqrt{s_{NN}} \leq 11.5$ GeV, the studied midrapidity range $|y| < 0.5$ is not a tiny fraction of the whole system, the hadron production in the midrapidity range may be influenced by effects of global charge conservation not only strangeness conservation but also baryon quantum number conservation. Therefore, grand-canonical treatment may be not perfectly suitable. We now consider the result of canonical ensemble for free quark system. We apply the method of canonical statistics [55] to obtain the property of quark number distribution under the constraint of finite baryon quantum number and strangeness. We put the detailed derivation into the Appendix. The inputs of canonical ensemble are volume V , temperature T , and charges (B, Q, S) . The temperature is set to the hadronization temperature whose values at different collision energies are taken as before. As discussions in Sec. III, we take $S = 0$. V , B , and Q can be determined by fitting the quark and antiquark numbers integrated from Fig. 2. Results of $\lambda_s^{(\text{CE})}$ for canonical ensemble of quark system are shown as solid circles with the dotted line in Fig. 13. We see that $\lambda_s^{(\text{CE})}$ is also increased with the decrease of collision energy and is smaller than $\lambda_s^{(\text{GCE})}$, in particular, at low collision energies. Our extracted λ_s is roughly located in the middle of two ensembles.

VII. SUMMARY AND DISCUSSIONS

In this paper, we have applied a quark combination model with equal-velocity combination approximation to systematically study the production of hadrons in Au+Au collisions at RHIC energies. The model applied in this work is motivated by our recent findings for the constituent quark number scaling property of hadronic p_T spectra in high-energy pp , pA and AA collisions [23,24,28]. After systematic study of p_T spectra and yields for hadrons, we found that our quark combination model provides a good explanation on the experimental data in Au+Au collisions at $\sqrt{s_{NN}} \geq 11.5$ GeV. This suggests that the constituent quark degrees of freedom still play important role even at low RHIC energy, which is closely related to the deconfinement at these collision energies.

By study of hadronic p_T spectra and yields in these collisions, we obtained p_T spectra and numbers of constituent quarks and antiquarks at hadronization. We calculated the net strangeness $N_{\bar{s}} - N_s$ at midrapidity and showed the strangeness neutralization is well satisfied at midrapidity in heavy-ion collisions at RHIC energies. We studied the spectrum ratio of strange quarks to newborn up/down quarks

$f_s(p_T)/f_{\bar{u}}(p_T)$ and the p_T integrated number ratio $\lambda_s = N_s/N_{\bar{u}}$ at different collision energies. We applied the basic thermal statistics for free constituent quark system to understand these properties of strange quarks relative to up/down quarks.

We emphasize the key physics in our model which are responsible for successfully explaining experimental data of hadronic p_T spectra and yields. First, the model takes the constituent quarks and antiquarks as the effective interface connecting the strongly-interacting system before hadronization and that after hadronization. We assume the constituent quarks and antiquarks as effective degrees of freedom for the strongly-interacting quark-gluon system just before hadronization. We take the constituent quark model to describe the static structure of hadrons in the ground state. In this scenario, the equal-velocity combination of these constituent quarks and antiquarks is a reasonable approximation and is indeed supported by the quark number scaling property for p_T spectra of hadrons observed in experiments [23,24,28]. The study in this paper further showed that the equal-velocity combination can systematically describe the production of different kinds of hadrons in heavy-ion collisions at RHIC energies. Second, the model includes reasonable considerations for the unity of hadronization and the linear response property, see detailed discussions in Ref. [36]. This is very important to reproduce the multihadron yield correlations shown in Fig. 10. For example, in a naive inclusive view of combination, we have $N_{\Omega} \propto N_s^3$ and $N_{\bar{\Omega}} \propto N_{\bar{s}}^3$ and therefore $\bar{\Omega}^+/\Omega^- \propto (N_{\bar{s}}/N_s)^3 \approx 1$ which is independent of collision energy. However, yield of Ω^- in our model is not only dependent on N_s^3 but also dependent on the global system information shown as in Eq. (17); thus, we have $\bar{\Omega}^+/\Omega^- = [(1-z)/(1+z)]^{a-3}$ in Eq. (51) which decreases with the decrease of collision energy.

To further test our EVC model, the following two aspects are deserved to study in depth in future works. The first is the effect of momentum correlations among quarks and antiquarks at hadronization. It is neglected in this paper; see Eqs. (5) and (6). In general, quarks and antiquarks at hadronization always have some momentum correlations. In heavy-ion collisions, the collective flow formed in parton phase will cause a certain correlation among momenta of quarks and antiquarks. This correlation not only influences the inclusive momentum spectra of hadrons to a certain extent but also influences multiparticle momentum correlations more directly. In the future work, we will study this effect by building sensitive physical observables in EVC model. The second is the production of short-lived resonances. In heavy-ion collisions, yield and momentum spectra of finally observed resonances such as $K^*(892)$ are strongly influenced by rescatterings among hadrons. In the future work, we will systematically consider this hadronic rescattering effect and study the production mechanism of the short-lived resonances at hadronization.

ACKNOWLEDGMENTS

This work is supported in part by the National Natural Science Foundation of China under Grant No. 11975011,

Shandong Province Natural Science Foundation under Grants No. ZR2019YQ06 and No. ZR2019MA053, and Higher Educational Youth Innovation Science and Technology Program of Shandong Province (Grants No. 2019KJJ010 and No. 2020KJJ004).

APPENDIX: QUARK NUMBER DISTRIBUTION IN CANONICAL ENSEMBLE

The probability of a single state in the canonical ensemble is

$$P_{\text{state}} = \frac{1}{Z(\mathbf{Q})} e^{-E_{\text{state}}\beta} \delta_{\mathbf{Q}, \mathbf{Q}_{\text{state}}}, \quad (\text{A1})$$

where $\beta = 1/T$ is the inverse temperature, E_{state} is the energy of the state and $\mathbf{Q}_{\text{state}}$ are Abelian charges of the state

$$\mathbf{Q}_{\text{state}} = \sum_{j=1}^K \mathbf{q}_j N_j. \quad (\text{A2})$$

Here N_j is the number of particle j in the current state and $\mathbf{q}_j = (B_j, Q_j, S_j)$ is the quantum number vector for the j th particle. K is the number of particle species.

The multiplicity distribution of particles can be obtained from the generating function associated to the canonical partition function $Z(\mathbf{Q})$ [55] and is expressed as

$$P(\{N_j\}) = \frac{1}{Z(\mathbf{Q})} \prod_{j=1}^K \left\{ \sum_{\{h_{n_j}\}} \prod_{n_j=1}^{N_j} \left[\frac{[z_j(n_j)]^{h_{n_j}}}{n_j^{h_{n_j}} h_{n_j}!} \right] \right\} \delta_{\mathbf{Q}, \sum_j \mathbf{q}_j N_j}, \quad (\text{A3})$$

where the summation takes different configurations for $\{h_{n_j}\}$ into account under the condition $\sum_{n_j=1}^{\infty} n_j h_{n_j} = N_j$:

$$z_j(n_j) = (\mp)^{n_j+1} \frac{gV}{(2\pi)^3} \int d^3 p e^{-n\beta E} = (\mp)^{n_j+1} gV \frac{m^2}{2\pi^2 n_j \beta} K_2(n_j \beta m). \quad (\text{A4})$$

Now, we consider the thermal system consisting of constituent quarks and antiquarks. In our quark combination model, constituent quarks and antiquarks are regarded as the effective degrees of freedom at hadronization and they freely combine to form baryons and/or mesons at hadronization. Therefore, we can simply apply above formula to obtain the number distribution of these ‘‘free’’ constituent quarks and antiquarks under canonical statistics. Here, we consider up, down, strange quarks and their antiparticles. Index j denotes $u, d, s, \bar{u}, \bar{d}, \bar{s}$, and $K = 6$.

Equation (A3) can be further denoted as

$$P(\{N_j\}) = \frac{1}{Z(\mathbf{Q})} \left[\prod_{j=1}^K \mathcal{Z}(S_{N_j}) \right] \delta_{\mathbf{Q}, \sum_j \mathbf{q}_j N_j}, \quad (\text{A5})$$

where $\mathcal{Z}(S_{N_j})$ is cycle-index polynomial of symmetric group. $\mathcal{Z}(S_{N_j})$ can be numerically evaluated using the recurrence

relation

$$\mathcal{Z}(S_N) = \frac{1}{N} \sum_{l=1}^N z(l) \mathcal{Z}(S_{N-l}), \quad (\text{A6})$$

with $\mathcal{Z}(S_0) = 1$ and $\mathcal{Z}(S_1) = z(1)$.

As discussed in Sec. III, we take strangeness neutralization $S = 0$ and therefore $N_s = N_{\bar{s}}$. For constraints of baryon charge B and electric charge Q , we denote them as $N_u - N_{\bar{u}} = B + Q$ and $N_d - N_{\bar{d}} = 2B - Q$. Finally, the joint distribution function of quark numbers and antiquark numbers is

$$P(N_d, N_u, N_s, N_{\bar{d}}, N_{\bar{u}}, N_{\bar{s}}) = \frac{1}{\mathcal{Z}(Q)} \mathcal{Z}(S_{N_d}) \mathcal{Z}(S_{N_{\bar{d}}}) \delta_{N_d, N_{\bar{d}}+2B-Q}$$

$$\begin{aligned} & \times \mathcal{Z}(S_{N_u}) \mathcal{Z}(S_{N_{\bar{u}}}) \delta_{N_u, N_{\bar{u}}+B+Q} \\ & \times \mathcal{Z}(S_{N_s}) \mathcal{Z}(S_{N_{\bar{s}}}) \delta_{N_s, N_{\bar{s}}}. \end{aligned} \quad (\text{A7})$$

We obtain the averaged number of quarks by

$$\bar{N}_s = \sum_{\{N_{q_i}\}} N_s P(N_d, N_u, N_s, N_{\bar{d}}, N_{\bar{u}}, N_{\bar{s}}), \quad (\text{A8})$$

$$\bar{N}_{\bar{u}} = \sum_{\{N_{q_i}\}} N_{\bar{u}} P(N_d, N_u, N_s, N_{\bar{d}}, N_{\bar{u}}, N_{\bar{s}}), \quad (\text{A9})$$

and calculate strangeness factor $\lambda_s^{(CE)} = \bar{N}_s / \bar{N}_{\bar{u}}$ in canonical ensemble of free quark system.

-
- [1] B. Andersson, G. Gustafson, G. Ingelman, and T. Sjostrand, *Phys. Rep.* **97**, 31 (1983).
- [2] B. Webber, *Nucl. Phys. B* **238**, 492 (1984).
- [3] K. P. Das and R. C. Hwa, *Phys. Lett. B* **68**, 459 (1977) [Erratum: **73**, 503 (1978)].
- [4] V. V. Anisovich and V. M. Shekhter, *Nucl. Phys. B* **55**, 455 (1973) [Erratum: **63**, 542 (1973)].
- [5] J. D. Bjorken and G. R. Farrar, *Phys. Rev. D* **9**, 1449 (1974).
- [6] Q.-B. Xie and X.-M. Liu, *Phys. Rev. D* **38**, 2169 (1988).
- [7] F. Becattini, *Z. Phys. C* **69**, 485 (1996).
- [8] P. Braun-Munzinger, J. Stachel, J. P. Wessels, and N. Xu, *Phys. Lett. B* **365**, 1 (1996).
- [9] V. Greco, C. M. Ko, and P. Lévai, *Phys. Rev. Lett.* **90**, 202302 (2003).
- [10] R. J. Fries, B. Müller, C. Nonaka, and S. A. Bass, *Phys. Rev. Lett.* **90**, 202303 (2003).
- [11] D. Molnar and S. A. Voloshin, *Phys. Rev. Lett.* **91**, 092301 (2003).
- [12] Z.-W. Lin and D. Molnar, *Phys. Rev. C* **68**, 044901 (2003).
- [13] F.-L. Shao, Q.-B. Xie, and Q. Wang, *Phys. Rev. C* **71**, 044903 (2005).
- [14] L.-W. Chen and C. M. Ko, *Phys. Rev. C* **73**, 044903 (2006).
- [15] A. Adare *et al.* (PHENIX Collaboration), *Phys. Rev. Lett.* **98**, 162301 (2007).
- [16] L. Adamczyk *et al.* (STAR Collaboration), *Phys. Rev. Lett.* **116**, 062301 (2016).
- [17] B. B. Abelev *et al.* (ALICE Collaboration), *J. High Energy Phys.* **06** (2015) 190.
- [18] S. Acharya *et al.* (ALICE Collaboration), *J. High Energy Phys.* **09** (2018) 006.
- [19] L. Adamczyk *et al.* (STAR Collaboration), *Phys. Rev. C* **88**, 014902 (2013).
- [20] K. Adcox *et al.* (PHENIX Collaboration), *Phys. Rev. Lett.* **88**, 242301 (2002).
- [21] B. Abelev *et al.* (STAR Collaboration), *Phys. Rev. Lett.* **97**, 152301 (2006).
- [22] B. B. Abelev *et al.* (ALICE Collaboration), *Phys. Rev. Lett.* **111**, 222301 (2013).
- [23] J. Song, X.-R. Gou, F.-L. Shao, and Z.-T. Liang, *Phys. Lett. B* **774**, 516 (2017).
- [24] J.-W. Zhang, H.-H. Li, F.-L. Shao, and J. Song, *Chin. Phys. C* **44**, 014101 (2020).
- [25] X.-R. Gou, F.-L. Shao, R.-Q. Wang, H.-H. Li, and J. Song, *Phys. Rev. D* **96**, 094010 (2017).
- [26] J. Song, H.-H. Li, and F.-L. Shao, *Eur. Phys. J. C* **78**, 344 (2018).
- [27] H.-H. Li, F.-L. Shao, J. Song, and R.-Q. Wang, *Phys. Rev. C* **97**, 064915 (2018).
- [28] J. Song, F.-L. Shao, and Z.-T. Liang, *Phys. Rev. C* **102**, 014911 (2020).
- [29] J. Adam *et al.* (STAR Collaboration), *Phys. Rev. C* **102**, 034909 (2020).
- [30] B. Buschbeck, H. Dibon, and H. R. Gerhold, *Z. Phys. C* **7**, 73 (1980).
- [31] Z.-T. Liang and Q.-B. Xie, *Phys. Rev. D* **43**, 751 (1991).
- [32] E. Braaten, Y. Jia, and T. Mehen, *Phys. Rev. Lett.* **89**, 122002 (2002).
- [33] J. Zimányi, T. S. Biró, T. Csörgő, and P. Lévai, *Phys. Lett. B* **472**, 243 (2000).
- [34] R. C. Hwa and C. B. Yang, *Phys. Rev. C* **67**, 034902 (2003).
- [35] F.-L. Shao, G.-J. Wang, R.-Q. Wang, H.-H. Li, and J. Song, *Phys. Rev. C* **95**, 064911 (2017).
- [36] J. Song and F.-L. Shao, *Phys. Rev. C* **88**, 027901 (2013).
- [37] J. Adam *et al.* (ALICE Collaboration), *Eur. Phys. J. C* **76**, 245 (2016).
- [38] S. Acharya *et al.* (ALICE Collaboration), *Phys. Lett. B* **807**, 135501 (2020).
- [39] D. Adamova *et al.* (ALICE Collaboration), *Eur. Phys. J. C* **77**, 389 (2017).
- [40] K. Olive *et al.* (Particle Data Group Collaboration), *Chin. Phys. C* **38**, 090001 (2014).
- [41] S. S. Adler *et al.* (PHENIX Collaboration), *Phys. Rev. C* **69**, 034909 (2004).
- [42] J. Adams *et al.* (STAR Collaboration), *Phys. Rev. Lett.* **98**, 062301 (2007).
- [43] B. I. Abelev *et al.* (STAR Collaboration), *Phys. Rev. C* **79**, 064903 (2009).
- [44] B. I. Abelev *et al.* (STAR Collaboration), *Phys. Rev. C* **79**, 034909 (2009).
- [45] M. M. Aggarwal *et al.* (STAR Collaboration), *Phys. Rev. C* **83**, 024901 (2011).
- [46] L. Adamczyk *et al.* (STAR Collaboration), *Phys. Rev. C* **96**, 044904 (2017).
- [47] L. Adamczyk *et al.* (STAR Collaboration), *Phys. Rev. C* **93**, 021903 (2016).

- [48] C.-E. Shao, J. Song, F.-L. Shao, and Q.-B. Xie, *Phys. Rev. C* **80**, 014909 (2009).
- [49] J. Adams *et al.* (STAR Collaboration), *Phys. Rev. Lett.* **92**, 182301 (2004).
- [50] K. Adcox *et al.* (PHENIX Collaboration), *Phys. Rev. Lett.* **89**, 092302 (2002).
- [51] I. Arsene *et al.* (BRAHMS Collaboration), *Phys. Lett. B* **687**, 36 (2010).
- [52] E. Schnedermann, J. Sollfrank, and U. W. Heinz, *Phys. Rev. C* **48**, 2462 (1993).
- [53] L.-X. Sun, R.-Q. Wang, J. Song, and F.-L. Shao, *Chin. Phys. C* **36**, 55 (2012).
- [54] F.-L. Shao, J. Song, and R.-Q. Wang, *Phys. Rev. C* **92**, 044913 (2015).
- [55] F. Becattini and L. Ferroni, *Eur. Phys. J. C* **38**, 225 (2004) [Erratum: **66**, 341 (2010)].